Dynamics of $He^{2+}+H(1s)$ excitation and electron-capture processes in Debye plasmas

L. Liu,[1] J. G. Wang,[1] and R. K. Janev[2]
[1]*Institute of Applied Physics and Computational Mathematics, P.O. Box 8009, Beijing 100088, People's Republic of China*
[2]*Macedonian Academy of Sciences and Arts, P. O. Box 428, 1000 Skopje, Macedonia*

(Received 16 September 2007; revised manuscript received 21 December 2007; published 14 March 2008)

Collision dynamics of the $He^{2+}+H(1s)$ system imbedded in a Debye plasma is studied by the two-center atomic orbital close-coupling (AOCC) method in the energy range 5–300 keV/u. The atomic orbitals and electron binding energies of atomic states are calculated within Debye-Hückel approximation of the screened Coulomb potential and used in AOCC dynamics formalism to calculate the state-selective electron capture and excitation cross sections. The basis contained 174 orbitals centered on the target (all $n \leq 6$ discrete states and 117 quasicontinuum states) and 20 orbitals centered on the projectile (all $n \leq 4$ discrete states). It is demonstrated that the screening of Coulomb interactions in the system progressively reduces the number of available excitation and electron capture channels when the screening parameter increases. The screening of Coulomb interactions introduces changes also in the values of direct and exchange couplings, thus affecting the magnitude and energy behavior of the cross sections. The control of dynamics of collision processes in a Debye plasma by varying the plasma screening of Coulomb interactions in the collision system is discussed.

DOI: 10.1103/PhysRevA.77.032709 PACS number(s): 34.20.Cf, 34.70.+e, 52.20.Hv

I. INTRODUCTION

Atomic collision processes in hot, dense plasmas have been subject to continuous interest during the last several decades ([1–4], and references herein). Most of this interest has been motivated by the spectroscopy of such plasmas [5,6] and, therefore, the electron-impact processes (excitation [2,7–11], ionization [12], and recombination [13]), involving hydrogenlike ions, have received the main attention. These studies have covered both weakly and strongly coupled plasmas. The electron-ion interaction in the case of weakly coupled plasmas is adequately described by the Debye-Hückel potential (with or without inclusion of dynamical plasma screening effects), while in the case of strongly coupled plasma the interaction is usually described by the ion-sphere model potential (see, e.g., [1,2]). To the best of our knowledge, the only studies involving heavy-particle collision processes in hot, dense plasmas are those for proton-impact excitation of $n=2$ fine-structure levels of hydrogenlike ions [14], electron capture in proton-hydrogenic ion collisions [15], symmetric resonant charge exchange in hydrogenlike ion-parent nucleus collisions [16], and the classical trajectory Monte Carlo study of electron capture and ionization in hydrogen atom and fully stripped ion collisions [17]. The transitions between the $n=2$ fine-structure levels in Ref. [14] have been calculated within a close-coupling scheme employing both the static Debye-Hückel and the ion-sphere model potentials. The electron capture process in Ref. [15] was described by the classical Bohr-Lindhard model [18] using, however, its high energy part only. While Ref. [15] used a Debye-Hückel potential for electron-ion interactions, in Ref. [16] the ion-sphere model potential was used for their description. We would like to note that in all the above mentioned studies, the change of the electronic bound state wave functions and energies in the screened Coulomb potential was taken into account at most within the first-order perturbation theory (e.g., in [14]). In Ref. [17], the microcanonical distribution for the bound $1s$ state of H was determined by using the Debye-Hückel potential and the accurate dependence of the energy of this state on the Debye screening length λ_D [19].

In the present work we shall study the excitation and electron capture processes in $He^{2+}+H(1s)$ collisions

$$He^{2+} + H(1s) \rightarrow He^{2+} + H(nl) \tag{1}$$

$$\rightarrow He^{+}(nl) + H^{+} \tag{2}$$

in a plasma in which the interaction of an electron with an ion of positive charge Z at a distance r is given by the Debye-Hückel potential (e is the unit charge)

$$V(r) = -\frac{Ze^2}{r} e^{-r/\lambda_D}, \tag{3}$$

where $\lambda_D=(k_B T_e/4\pi e^2 n_e)^{1/2}$ is the Debye screening length, T_e and n_e are the plasma electron temperature and density, respectively, and k_B is the Boltzmann constant. In the theory of electrolyte fluids [20], the screened Coulomb potential (3) results from the linearization of the Poisson-Boltzmann equation and accounts only for the pair correlations in the many-body system of charged particles. In the context of fully ionized plasmas it derives from the second equation of BBGKY hierarchy in the pair correlation approximation (see, e.g., [21]). The representation of charged particle interaction in a plasma by the potential (3) is adequate only if the Coulomb coupling parameter $\Gamma=e^2/(ak_B T_e)$ and plasma nonideality parameter $\gamma=e^2/(\lambda_D k_B T_e)$ satisfy the conditions $\Gamma \leq 1$, $\gamma \ll 1$, where $a=[3/(4\pi n_e)]^{1/3}$ is the average interparticle distance. There is a wide class of laboratory and astrophysical plasmas in which these conditions are fulfilled (Debye plasmas). In particular, the inertial confinement fusion plasmas with parameters $T_e \sim 1-10$ keV and $n_e \sim 1-10\times 10^{24}$ cm^{-3} belong to this type of plasma.

We shall study the dynamics of processes (1) and (2) by employing the two-center atomic orbital close-coupling (TC-AOCC) method [22] with plane wave electron translational

factors (PW ETFs) in the energy range 5–300 keV/u. The atomic orbitals have been determined variationally from the corresponding single-center Schrödinger equation with the potential (3). The employed AO basis included 174 orbitals centered on the target (all $n \leq 6$ and $7s$ discrete states and 117 quasicontinuum states) and 20 states centered on the projectile (all $n \leq 4$ discrete states) were sufficient to ensure reliable results both in the unscreened and screened interaction cases. The main objective of the present study is to explore how the screened Coulomb interaction (3) affects the dynamics of processes (1) and (2) when the Debye screening length λ_D varies. The results presented below show that the variation of λ_D has dramatic effects on the collision dynamics, controlling the number of reaction channels in processes (1) and (2) and the magnitude and energy behavior of the cross sections of the open channels. There have been many theoretical studies in the past of processes (1) and (2) with pure Coulomb interactions between the particles. The most comprehensive ones, in terms of the size of the expansion basis, are the TC-AOCC calculations in Refs. [23–25], the triple-center expansion calculations in Ref. [26], and the molecular-orbital close-coupling (MOCC) calculations in Ref. [27].

The paper is organized as follows. In the next section we briefly outline the theoretical method used in the cross section calculations, with emphasis on the specific features that the screened Coulomb potential (3) introduces in the AO basis and dynamical couplings. In Sec. III we present the results of state-selective cross sections for processes (1) and (2), and in Sec. IV we give our conclusions. Atomic units will be used in the remaining part of this paper, unless explicitly indicated otherwise.

II. THEORETICAL METHOD

A. Atomic orbitals and energies of screened Coulomb potential

The application of the TC-AOCC method to an ion-atom collision system requires determination of single-center electronic states over which the total scattering wave function is expanded and used in a time-dependent Schrödinger equation to generate the coupled equations for the state amplitudes [22]. For determining the stationary bound electronic states with the potential (3) centered on the target ($Z=1$) and on the projectile ($Z=2$), we have used the variational method with the even-tempered trial functions [25,28]

$$\chi_{klm}(\vec{r};\lambda_D) = N_l(\xi_k(\lambda_D))r^l e^{-\xi_k(\lambda_D)r} Y_{lm}(\hat{\vec{r}}),$$

$$\xi_k(\lambda_D) = \alpha\beta^k, \quad k = 1,2,\ldots,N, \tag{4}$$

where $N_l(\xi_k)$ is a normalization constant, $Y_{lm}(\hat{\vec{r}})$ are the spherical harmonics, and α and β are variational parameters, determined by minimization of the energy for each value of λ_D. The atomic states $\phi_{nlm}(\vec{r};\lambda_D)$ are then obtained as linear combination

$$\phi_{nlm}(\vec{r};\lambda_D) = \sum_k c_{nk}\chi_{klm}(\vec{r};\lambda_D), \tag{5}$$

where the coefficients c_{nk} are determined by diagonalization of single-center Hamiltonian. This diagonalization yields the energies $E_{nl}(\lambda_D)$ of the bound states in the screened Coulomb potential (3).

It is well known (see, e.g., [29]) that any attractive central-symmetric potential that at $r \to \infty$ decreases faster than $-r^{-2}$ supports a finite number of bound states. For any finite value of λ_D, the potential (3) belongs to this class of potentials. Moreover, for any finite value of λ_D, the high internal (dynamic) symmetry of the Coulomb field is reduced which results in lifting the l degeneracy of Coulomb energy levels. It is obvious that with increasing the screening of Coulomb potential (decreasing λ_D), the number of bound states, N_b, supported by the potential (3) will decrease, implying that the bound n, l states will successively enter the continuum with decreasing λ_D. There have been many calculations in the past of the energies $E_{nl}(\lambda_D)$ of hydrogenlike systems employing the perturbation (e.g., [30,31], and references therein) and variational (e.g., [19,32,33]) methods, as a well as a numerical solution of the Schrödinger equation [34,35]. These calculations indeed show that for each n, l state, the corresponding energy $E_{nl}(\lambda_D)$ becomes zero at certain critical screening length $\lambda_{D,c}^{n,l}$. For a given l, $\lambda_{D,c}^{n,l} < \lambda_{D,c}^{n+1,l}$, and for a given n, $\lambda_{D,c}^{n,l} < \lambda_{D,c}^{n,l+1}$. The number of bound n, l states in the screened Coulomb potential (3) for a given value of λ_D is $N_b = 0.583 + 0.499Z\lambda_D$ [34,35].

In Fig. 1 we show the λ_D dependence of the energies E_{nl} of the first six states of the hydrogen atom [panel (a)] and the He^+ ion [panel (b)] calculated by the above outlined variational procedure. The dashed lines in Fig. 1(a) represent the results of a numerical solution of a Schrödinger equation [35], indicating the good accuracy of present calculations. It is to be noted in Fig. 1 that the considered $n \leq 3$ energy levels rapidly approach the continuum edge for λ_D below $20-30a_0$, the gradient increasing with increasing n and l. The energy difference $\Delta E_{n,l;n+1,l\pm k} = E_{n,l} - E_{n+1,l\pm k}$ ($k = 0,1,2,\ldots$) decreases with decreasing λ_D, particularly for $\Delta E_{n,l;n+1,l-k}$, and for $n \leq 7$ some of the $E_{n+1,l-k}$ energies may cross with $E_{n,l}$ levels [35]. All these features of $E_{nl}(\lambda_D)$ energy levels, exhibited with varying the screening length λ_D, have important spectroscopic consequences.

In Tables I and II we give the values of $\lambda_{D,c}^{n,l}$ for the $n \leq 5$ states in H and He^+, respectively. In Table I the corresponding $\lambda_{D,c}^{n,l}$ values from Ref. [35] are also shown (in parentheses) for comparison. It can be observed from this table that the accuracy of our variational calculations in determining the values $\lambda_{D,c}^{n,l}$ (as well as the values of $E_{n,l}$ for λ_D close to $\lambda_{D,c}^{n,l}$) for $n \geq 4$ deteriorates, especially for the lower l sublevels. With increasing the distance $\lambda_D - \lambda_{D,c}^{n,l}$, the difference between variationally calculated and exact $E_{n,l}$ values become much smaller, and can be further decreased by choosing more variational parameters in the trial functions. However, for the purposes of the present work, the main objective of which is to show the principle effects of the screened Coulomb interactions on the collision dynamics, these small differences are unessential (see also Sec. II B).

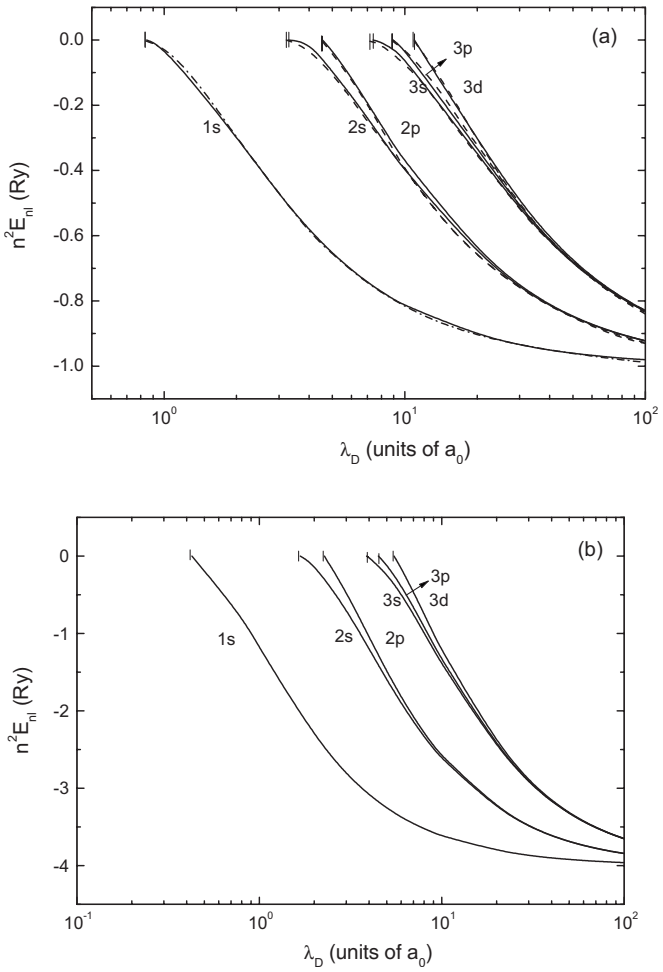

FIG. 1. Dependence of binding energies on λ_D of the $n \leq 3$ state of H (a) and He^+ (b). The dashed lines in (a) are the results of Ref. [35].

In Figs. 2(a) and 2(b) we show the radial electron density distributions of H $(1s)$ and $He^+(2p)$ states for a number of values of Debye length λ_D and for the unscreened case. It can be seen from these figures that despite the significant changes of the energies of these two states with decreasing λ_D [see Figs. 1(a) and 1(b)], their radial density distributions exhibit significant changes only when λ_D becomes close enough to the corresponding $\lambda_{D,c}^{n,l}$ value (cf. Tables I and II). One should, however, note that with decreasing λ_D the distribution becomes broader, its peak is shifted towards larger radial distances, and its magnitude decreases.

B. TC-AOCC coupled equations

Within the semiclassical approximation, the electron wave function of the $He^{2+}+H(1s)$ collision system $\Psi(\vec{r},t)$ satisfies the equation

$$\left(H - i\frac{\partial}{\partial t}\right)\Psi(\vec{r},t) = 0, \tag{6}$$

where

$$H = -\frac{1}{2}\nabla_r^2 + V_A(r_A) + V_B(r_B), \tag{7}$$

and $V_{A,B}(r_{A,B})$ are the electron interactions with the target proton (subscript A) and projectile ion He^{2+} (subscript B) of the form (3). In the collision energy range considered in the present paper (5–300 keV/u), the straight-line approximation for the relative nuclear motion, $\vec{R}(t)=\vec{b}+\vec{v}t$ (b is the impact parameter and v is the collision velocity), can be safely adopted [22] (even more justifiably than in the pure Coulomb case since the nucleus-nucleus interaction is also screened). Expanding the wave function $\Psi(\vec{r},t)$ in terms of bound atomic orbitals (5), multiplied by plane wave ETFs [22] [then giving "traveling" atomic orbitals $\phi(\vec{r},t;\lambda_D)$]

$$\Psi(\vec{r},t) = \sum_i a_i(t)\phi_i^A(\vec{r},t;\lambda_D) + \sum_j b_j(t)\phi_j^B(\vec{r},t;\lambda_D), \tag{8}$$

and inserting it into Eq. (6), one obtains the system of coupled equations for the amplitudes $a_i(t)$ and $b_j(t)$ [22],

$$i(\dot{A} + S\dot{B}) = HA + KB, \tag{9a}$$

$$i(\dot{B} + S^\dagger\dot{A}) = \bar{K}A + \bar{H}B, \tag{9b}$$

where A and B are the vectors of amplitudes a_i $(i=1,2,\ldots)$ and b_j $(j=1,2,\ldots)$, respectively, S is the overlap matrix ($S^\dagger$ is its transposed form), H and $\bar{H}$ are direct cou-

TABLE I. Critical screening lengths, $\lambda_{D,c}^{n,l}(a_0)$, for H (nl) states, $n \leq 5$.

n/l	0	1	2	3	4
1	0.8450 (0.8399)[a]				
2	3.280 (3.223)	4.542 (4.541)			
3	7.380 (7.171)	8.900 (8.872)	10.950 (10.947)		
4	12.750 (12.687)	14.980 (14.731)	17.250 (17.210)	20.080 (20.068)	
5	21.260 (19.772)	23.550 (22.130)	25.400 (24.985)	28.550 (28.257)	34.600 (31.904)

[a]The values in parentheses are from Ref. [35].

TABLE II. Critical screening lengths, $\lambda_{D,c}^{n,l}(a_0)$, for He^+ (nl) states, $n \leq 5$.

n/l	0	1	2	3	4
1	0.42715				
2	1.67800	2.2725			
3	3.87300	4.4920	5.4817		
4	7.39500	7.8690	8.8520	10.120	
5	14.2800	14.045	15.015	16.020	17.415

pling matrices on the target and projectile, respectively, and K and $\bar{K}$ are the electron exchange matrices. The system of equations (9) is to be solved under the initial conditions

$$a_i(-\infty) = \delta_{1i}, \quad b_j(-\infty) = 0. \tag{10}$$

After solving the system of coupled equations (9), the cross section for $1 \rightarrow i$ excitation and $1 \rightarrow j$ electron-capture transitions are calculated as [22]

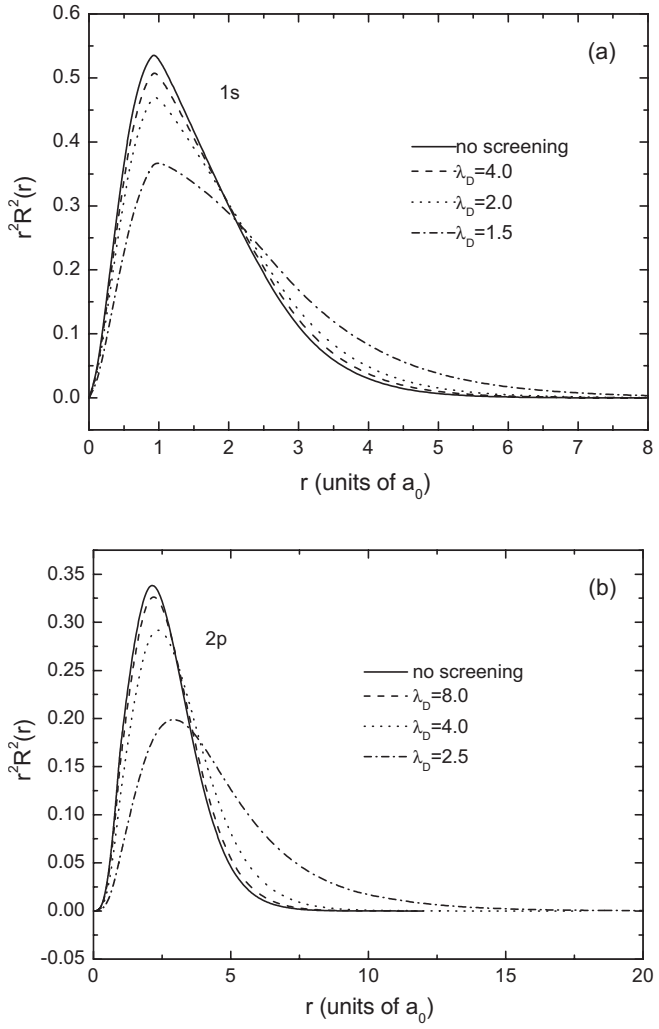

FIG. 2. Electron density distribution of H$(1s)$ (a) and $He^+(2p)$ (b) states for a number of λ_D values.

$$\sigma_{exc,i} = 2\pi \int_0^\infty |a_i(+\infty)|^2 b db, \tag{11}$$

$$\sigma_{cx,j} = 2\pi \int_0^\infty |b_j(+\infty)|^2 b db. \tag{12}$$

The sums of $\sigma_{exc,i}$ over i and $\sigma_{cx,j}$ over j give the corresponding total excitation and electron-capture (charge exchange) cross section, respectively.

One of the important differences of the AOCC description of atomic processes in the discrete spectrum with screened Coulomb interactions with respect to the unscreened case is that the number of states in the discrete spectrum on each of the screened Coulomb centers is always finite and uniquely defined by the value of the screening length λ_D. For instance, from Tables I and II one can see that for $\lambda_D \leq 14.0a_0$, only the states with $n \leq 4$ are in the discrete spectrum of He^+ and only the $4s$ and $n \leq 3$ states are in the discrete spectrum of H. While the relation $N_b = 0.583 + 0.499Z\lambda_D$ determines the number of bound states on the center with charge Z for a given value of λ_D and, thereby, the reaction channels involved in their population, the dependence of the atomic orbitals on λ_D affects the couplings between the states remaining in the discrete spectrum for a given λ_D, and thereby the dynamics.

In Figs. 3(a) and 3(b) we show the dependence on internuclear distance R of matrix elements for direct $1s \rightarrow 2s$ and $1s \rightarrow 2p$ transitions in H for the unscreened case and for the screened Coulomb interactions with several values of λ_D. We observe a rapid decrease of absolute values of these transition matrix elements with decreasing λ_D.

In Figs. 4(a) and 4(b) we show the R dependence of absolute values of $1s(H) \rightarrow 2s(He^+)$ and $1s(H) \rightarrow 2p(He^+)$ electron exchange matrix elements (calculated for $E = 25$ keV/u) for the unscreened case and for the screened interactions with $\lambda_D = 8.0$, 4.0, and $2.5a_0$. Again, a significant decrease of the values of these couplings is observed when λ_D decreases.

III. RESULTS OF CROSS SECTION CALCULATIONS

A. Excitation

Although the main purpose of the present work is to investigate the effects of the screening of Coulomb potential on the dynamics of the $He^{2+} + H(1s)$ collision system, we have nevertheless included in the expansion basis all the $n \leq 3$ and $7s$ discrete states and 117 continuum pseudostates (in total 174 states) on H and all the $n \leq 4$ states (in total 20

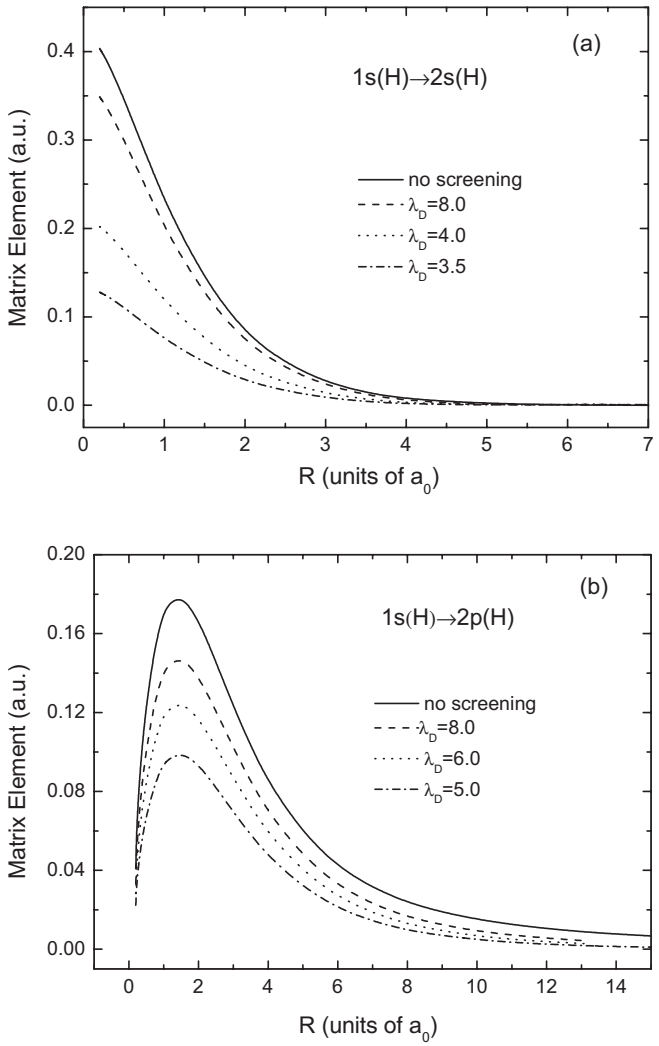

FIG. 3. Variation of matrix elements for direct $1s \rightarrow 2s$ (a) and $1s \rightarrow 2p$ (b) transitions in H at a number of λ_D values and for the unscreened case.

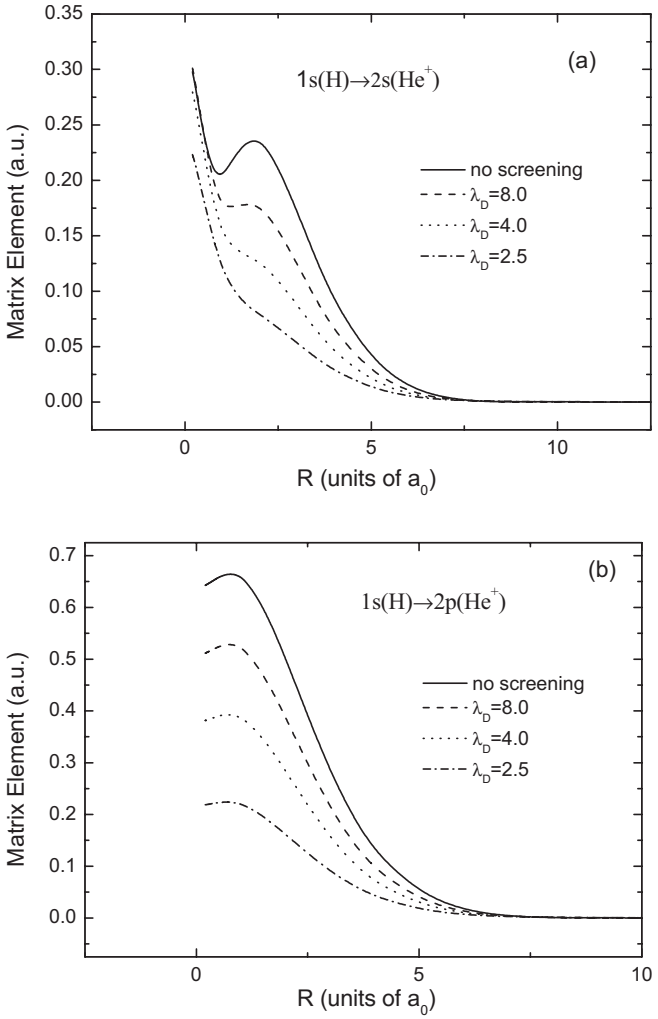

FIG. 4. Variation of absolute values of matrix elements for $H(1s) \rightarrow He^+(2s)$ (a) and $H(1s) \rightarrow He^+(2p)$ (b) electron exchange transitions for the unscreened case and for the screened cases with $\lambda_D = 8.0$, 4.0, and $2.5a_0$.

states) on He^+ in order to ensure the reliability of our results. A similarly large basis for the excitation, electron capture, and ionization studies in this collision system was used in Ref. [25], where (the same) 174 states were centered on H and 35 discrete states (all states with $n \leq 5$) were centered on He^+. We denote these two basis sets as He20/H174 and He35/H174, respectively.

In order to investigate the sensitivity of the results on the size of the basis, we have performed $2s$ and $2p$ excitation cross section calculations for the unscreened and screened (with $\lambda_D = 6a_0$) cases for energies of 10 and 100 keV/u for three basis sets: He20/H10, He20/H174, and He35/H174. The results are shown in Table III. While the convergence of the basis set used in the present calculations is quite good in both the screened and unscreened case, the basis set He20/H10 is obviously insufficient to describe adequately the excitation to these two states. Note that for the $\lambda_D = 6a_0$ screening the only discrete excited states centered on H are the $2s$ and $2p$ states. The large disagreement of $2s$ and $2p$ excitation cross sections of the He20/H10 basis with those of the He20/H174 basis in the $\lambda_D = 6a_0$ case indicates the important role of the coupling with the quasicontinuum states in the screened case.

In Figs. 5(a) and 5(b) we present the λ_D dependence of $2l$ and $3l$ excitation cross sections for the collision energies of 25 keV/u [panel (a)] and 100 keV/u [panel (b)] in the region $\lambda_D \leq 15a_0$. The expected sharp decrease of nl-excitation cross sections when λ_D approaches the critical value $\lambda_{D,c}^{n,l}$ is evident in these figures. It is, however, worth noting that this decrease is much sharper for the $l \geq 1$ states than for the ns states. This can be correlated with the large gradients of $E_{nl}(\lambda_D)$ curves for the $l \geq 1$ states near the continuum edge. The predominance of the $2p$ excitation channel at both these energies is also not surprising. The appearance of a maximum in the λ_D dependence of the $2p$ cross section for $E = 25$ keV/u might be partly related to the decrease of energy difference between $1s$ and $2p$ states and partly to the coupling with other states. Further, these figures show that by selecting the value of screening length λ_D in the range $3-11a_0$, one can select the open excitation channels.

The energy behavior of excitation cross sections is shown in Fig. 6 for the unscreened interactions [panel (a)] (only the

TABLE III. Comparison of excitation cross sections (in units of 10^{-16} cm^2) for the unscreened and $\lambda_D = 6a_0$ screened cases at $E=10$ and 100 keV/u for the He20/H174, He35/H174, and He20/H10 AO basis sets.

No screening	E (keV/u)	$2s$	$2p$
	10	0.08667	0.24184 (He20/H174)
		0.08588	0.23690 (He35/H174)
		0.05172	0.18181 (He20/H10)
	100	0.28113	1.77517 (He20/H174)
		0.27957	1.77460 (He35/H174)
		0.43641	2.30923 (He20/H10)
Screening with $\lambda_D=6a_0$	E (keV/u)	$2s$	$2p$
	10	0.10936	0.20103 (He20/H174)
		0.11148	0.20113 (He35/H174)
		0.08638	0.13466 (He20/H10)
	100	0.13239	0.97607 (He20/H174)
		0.13098	0.97560 (He35/H174)
		0.18622	1.28453 (He20/H10)

excitation to $n \leq 3$ states is shown) and for screened interactions with $\lambda_D=12a_0$ [panel (b)], $6.0a_0$ [panel (c)], and $4.0a_0$ [panel (d)]. The total (summed up) cross sections are also shown. In Fig. 6(a) we also show the cross-section data for $2s$ and $2p$ excitation of Ref. [25] (crosses), obtained with the He35/H174 basis. This further illustrates the accuracy of the present calculations.

In the screened case with $\lambda_D=12a_0$, only the states with $n \leq 3$ lie in the discrete part of the spectrum of H. The total excitation cross section in the screened case is only slightly reduced with respect to the unscreened case, but the changes in the $3l$ excitation cross sections are significant. These changes can be attributed to the changes of corresponding couplings for $\lambda_D=12a_0$. In the cases of screening with $\lambda_D=6.0a_0$ [panel (c)] and $\lambda_D=4.0a_0$ [panel (d)], only the states $2l$ and $2s$, respectively, remain in the discrete spectrum of H. The observed changes in the magnitude and energy behavior of $2s$ and $2p$ excitation cross sections with respect to the unscreened case, or the $\lambda_D=12a_0$ screened case, can again be attributed to the changes in the couplings [both the direct and exchange ones, the latter diverting the $n=2$, 3 capture flux back to the H ($n=2$) levels].

It is observed in Figs. 6(a)–6(d) that all cross sections, in both the unscreened and screened cases, exhibit an oscillatory structure in the energy region below ~20 keV/u. This structure is different for the states with different l, but remains λ_D invariant. The same oscillatory structure has been observed in the $n=2$ and $n=3$ excitation cross sections in TC-AOCC calculations of Ref. [23] (with a basis of 54 states) and in the MOCC calculations of Ref. [27] (with a basis of 83 states).

The observed quasi-independence of the positions of secondary peaks on the energy scale for excitation of $n=2$ and $n=3$ states on the size of the AO or MO basis (as long as the basis contains these states on H and He^+, and the $4s$ state on He^+) indicates that the mechanisms responsible for these

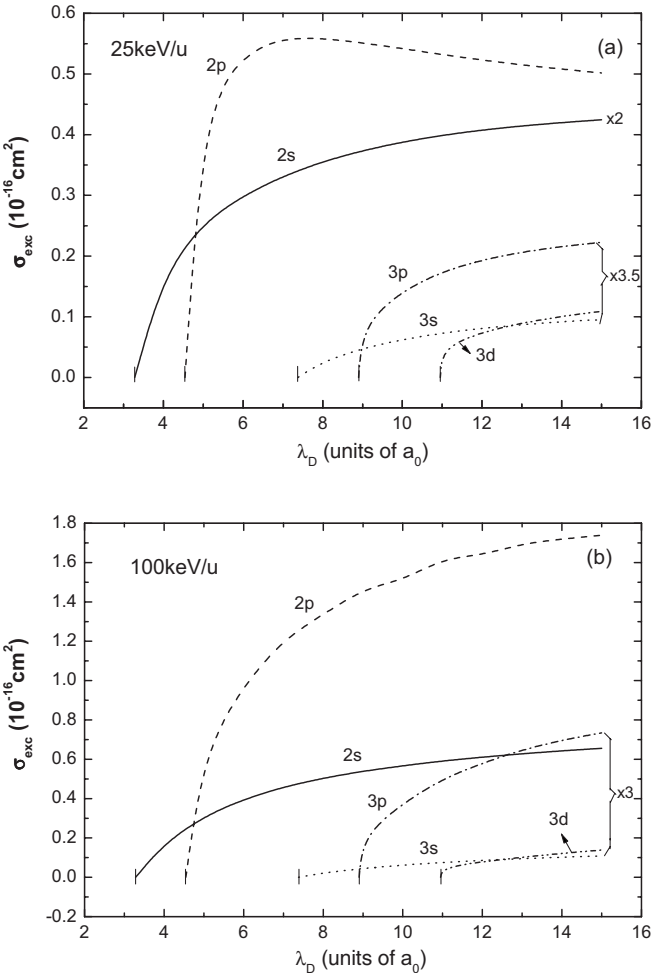

FIG. 5. λ_D dependence of excitation cross sections for $2l$ and $3l$ states of H for collision energies of 25 keV/u (a) and 100 keV/u (b).

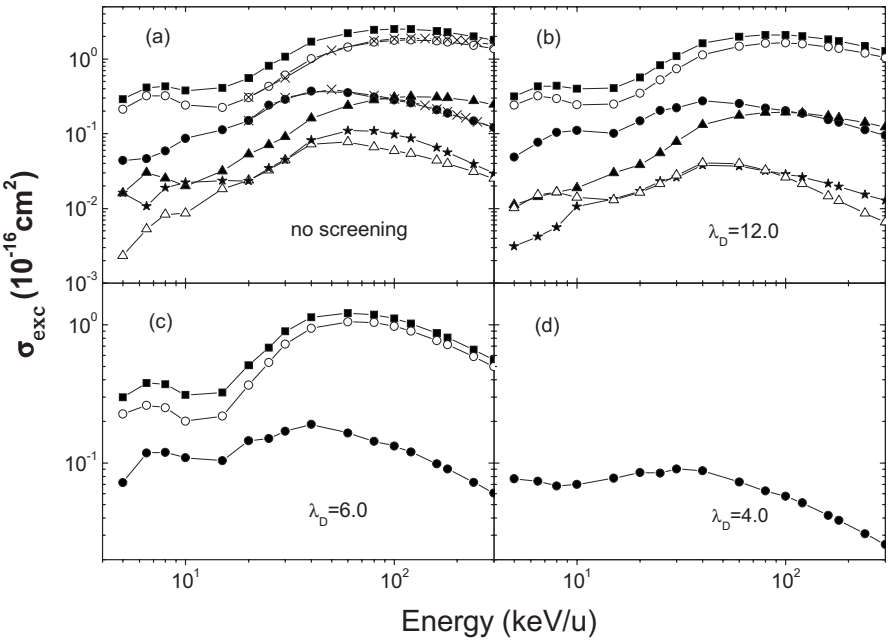

FIG. 6. Energy behavior of $2l$ and $3l$ excitation cross sections and their sum for the unscreened case (a) and screened cases with $\lambda_D=12a_0$ (b); $\lambda_D=6.0a_0$ (c); $\lambda_D=4.0a_0$ (d). The symbols are total cross section: filled squares; $2s$: filled circles; $2p$: open circles; $3s$: open triangles; $3p$: filled triangles; and $3d$: filled stars. The lines connecting the calculated data are to guide the eye. The crosses on $2s$ and $2p$ excitation curves in panel (a) are the data of Ref. [25] with a He35/H174 AO basis.

structures are confined within the couplings of these lower states. Indeed, a more detailed analysis of the couplings between the He^+ ($n=2$, 3) and H ($n=2$) states, as well as cross-section calculations with inclusion and exclusion of He^+ ($n=2$, 3) states from the basis, reveals that the origin of the structures in the $2s$ and $2p$ excitation cross sections is the back capture of the electron from the He^+ ($n=2$, 3) capture states to the H ($n=2$) states. A similar analysis reveals that the oscillations in the $3l$ excitation cross sections is due to the back capture from the He^+ ($n=3$, 4) states. In a molecular picture of collision dynamics of the $He^{2+}+H$ system in this low-energy collision region, the oscillations in the $2l$ and $3l$ excitation cross sections is a result of the phase interference of the coupled molecular states that asymptotically converge to the H ($n=2$, 3) and He^+ ($n=2$, 3, 4) atomic states (see, e.g., [36,37]).

B. Electron capture

The sensitivity of the electron-capture cross section results to the size of the basis for the unscreened and screened ($\lambda_D=4a_0$) cases is shown in Table IV for energies of 10 and 100 keV/u. The state-selective cross sections calculated with three basis sets, He20/H174, He35/H174, and He20/H10, are shown in the table. In the zero-screening case, the results of our He20/H174 basis show good convergence to the results of the He35/H174 basis for both collision energies. As expected from the analyses and calculations of Ref. [25], even the much more restricted basis He20/H10 can provide an acceptable description of electron-capture dynamics in the unscreened case. However, for the case of relatively strong interaction screening ($\lambda_D=4a_0$) the convergence is slower, especially at the lower collision energy and for the higher nl states. Noting that for $\lambda_D=4a_0$ screening the $1s$, $2l$, and $3s$ states are the only bound states on He^+, the relatively strong dependence of the high nl capture cross sections at low energies on the basis size indicates the importance of the coupling with the quasicontinuum states.

The selectivity in the population of electron-capture channels in reaction (2) with varying the Debye length λ_D can be inferred already from Fig. 1(b) and Table II. In Figs. 7(a) and 7(b) we show the electron-capture cross sections to the $2l$ and $3l$ states of He^+ as a function of λ_D for two collision energies: 25 keV/u [panel (a)] and 100 keV/u [panel (b)]. As in the case of excitation, with decreasing λ_D, the nl-capture cross sections, generally, decrease first gradually and then sharply when approaching the corresponding critical value $\lambda_{D,c}^{n,l}$, particularly for $l>0$ states. The dominant population of the $2p$ capture state for $\lambda_D \geq 2.5-3.0a_0$ is evident at both collision energies and is the result of the large value of the $1s$(H)-$2p$(He^+) electron exchange coupling [see Fig. 4(b)].However, at the higher energies (e.g., above 150 keV/u) the momentum transfer starts also to play an important role in the electron transfer dynamics (see, e.g., [22]) and the relative magnitude of the state-selective cross section is not anymore decisively determined by the electron exchange couplings. Therefore, at $E=100$ keV/u, the capture to the $1s$ state is comparable to that to the $2p$ state [cf. Fig. 7(b)].

The cross sections for electron capture to $1s$, $2s$, and $2p$ states in the zero-screening case are shown in Fig. 8 and compared with the results of He35/H174 calculations of Ref. [25] (denoted by crosses). In the overlapping energy range (20–250 keV/u) the results of present calculations practically coincide with those of Ref. [25]. The cross sections for capture to the higher nl states also have the same level of

TABLE IV. Comparison of electron-capture cross sections (in units of 10^{-16} cm^2) for the unscreened and $\lambda_D=4a_0$ screened cases at $E=10$ and 100 keV/u for the He20/H174, He35/H174, and He20/H10 AO basis sets.

No screening	E (keV/u)	$1s$	$2s$	$2p$	$3s$	$3p$	$3d$
	10	0.01502	2.24812	9.89382	0.11721	0.34453	0.42521 (He20/H174)
		0.01492	2.25318	9.90083	0.12129	0.34895	0.42207 (He35/H174)
		0.00732	2.32916	9.84436	0.12093	0.28395	0.40844 (He20/H10)
	100	0.10772	0.08683	0.14187	0.05325	0.06400	0.01544 (He20/H174)
		0.10742	0.08738	0.14109	0.05242	0.06451	0.01571 (He35/H174)
		0.09051	0.10100	0.16643	0.05793	0.07882	0.01383 (He20/H10)
Screening with $\lambda_D=4a_0$		E(keV/u)		$1s$	$2s$	$2p$	$3s$
		10		0.01944	1.47110	7.60813	0.04408 (He20/H174)
				0.01965	1.47736	7.67233	0.03716 (He35/H174)
				0.01093	1.23986	7.97528	0.03114 (He20/H10)
		100		0.10227	0.04499	0.08664	0.00484 (He20/H174)
				0.10157	0.04455	0.08402	0.00480 (He35/H174)
				0.08756	0.05398	0.12823	0.00417 (He20/H10)

mutual agreement, as illustrated in Table IV for the $3l$ states at $E=10$ and 100 keV/u.

In Figs. 9(a)–9(d) we show the nl-capture cross sections for the screened interactions with $\lambda_D=6.0$, 4.0, 2.0, and $1.5a_0$ [panels (a)–(d), respectively]. For $\lambda_D=6.0a_0$, the discrete spectrum of He^+ contains only the $n\leq 3$ states. Just as in the case of unscreened Coulomb potentials (see Fig. 8), the population of the $2p$ electron-capture channel dominates up to ~125 keV/u, from where on the population of the He^+ $(1s)$ state becomes dominant. The fact that the crossover of $2p$ and $1s$ capture cross sections at ~125 keV/u remains the same for $\lambda_D=6.0a_0$ and $\lambda_D=4.0a_0$ [cf. Figs. 8(a) and 8(b)], as well as in the unscreened case (see Fig. 8), is a clear indication that the momentum transfer becomes the dominant factor in the electron-capture dynamics at this and at higher collision energies.

In the $\lambda_D=4.0a_0$ screening case [Fig. 9(b)] only the $n\leq 2$ and $3s$ states remain in the discrete spectrum of He^+. While the magnitude and energy behavior of the cross sections for $n\leq 2$ states are not significantly changed with respect to the $\lambda_D=6.0a_0$ case, the reduction of the $3s$ cross-section magnitude is significant. The analysis of the couplings indicates that in the $\lambda_D=6.0a_0$ case the $He^+(3s)$ state is significantly populated via its interaction with the $He^+(3p)$ and $He^+(3d)$ states, which in the $\lambda_D=4.0a_0$ case are absent in the He^+ spectrum.

In the $\lambda_D=2.0a_0$ and $\lambda_D=1.5a_0$ screening cases [Figs. 9(c) and 9(d)] only the $1s$, $2s$, and $1s$ states are left in the He^+ spectrum, respectively. While the observed reduction of the $2s$ capture cross section with respect to its values in the $\lambda_D=4.0a_0$ case is due to the lack of its population via the $2p$ state (now absent in the He^+ spectrum), the relative small changes in the magnitude and energy behavior of the $1s$ capture cross section indicates that the population of $He^+(1s)$ is dominated by the $H(1s)-H^+(1s)$ exchange coupling (and the momentum transfer at high energies).

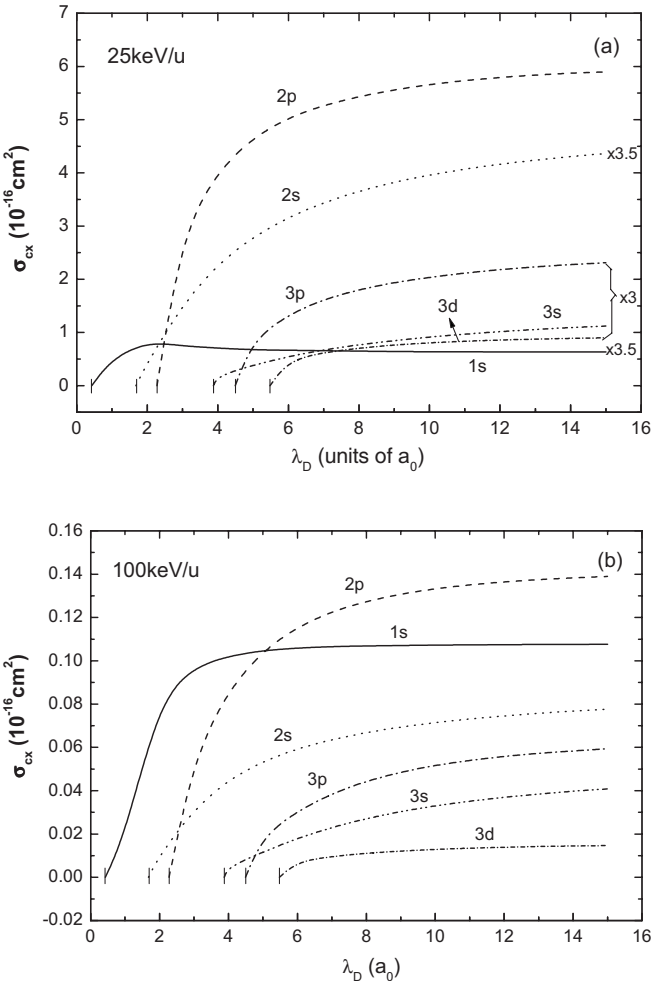

FIG. 7. λ_D dependence of electron-capture cross sections to $2l$ and $3l$ states of He^+ for collision energies of 25 keV/u (a) and 100 keV/u (b).

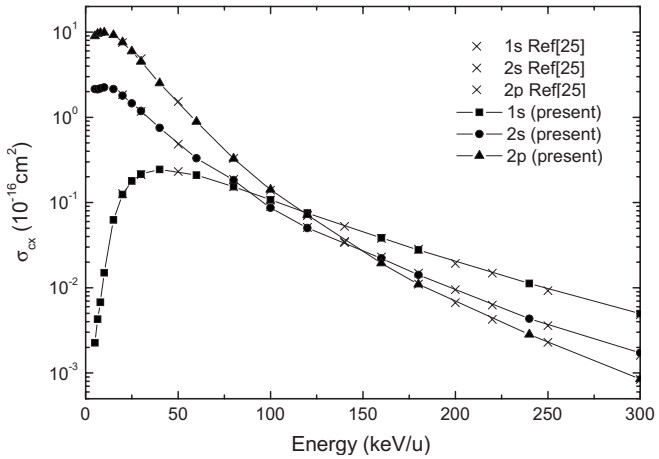

FIG. 8. Cross sections for electron capture to $1s$, $2s$, and $2p$ states of He^+. Crosses are the results of Ref. [25] performed with a He35/H174 AO basis.

In Fig. 10 we show the total electron-capture cross sections for the unscreened case and for the screened cases with $\lambda_D=12.0$, 6.0, 4.0, 2.5, 2.0, and $1.5a_0$. The reduction of total cross sections with increasing the screening, as well as the change of cross section energy behavior for $\lambda_D=2.0$ and $1.5a_0$ in the region below ~30 keV/u, is mainly due to the reduction of electron-capture channels with decreasing λ_D. We also note that for $\lambda_D<2.5a_0$ the coupling with the continuum of $2s$ and $1s$ discrete states becomes strong and at low collision energies (long interaction time) ionization from these states is expected to be strongly enhanced. The peculiar form of the total capture cross section for the $\lambda_D=2.0a_0$ case reflects just the displaced maxima of the contributing $2s$ and $1s$ capture cross section on the energy scale. The appearance of the mild shoulder in the $1s$ capture cross section at $E \sim 8$ keV/u can be attributed to the lost coupling of $1s$ with the $2s$ state when λ_D becomes less than $1.678a_0$, the Debye length value at which the $He^+(2s)$ state enters the continuum.

IV. CONCLUSIONS

In the present work we have investigated the dynamics of excitation and electron-capture processes in the $He^{2+}+H(1s)$ collision system with screened Coulomb interactions of type (3). The collision dynamics in the energy range 5–300 keV/u was described by the TC-AOCC method. We have demonstrated that the screening of Coulomb interactions in the $He^{2+}+H(1s)$ collision system introduces significant changes in its dynamics with respect to the unscreened case. The screening of Coulomb interactions affects the collision dynamics in three fundamental ways: (i) reduction of the number of states in the discrete spectrum of the target and projectile system, thus limiting the number of inelastic reaction channels; (ii) change (decrease) of energies of bound states (as well as their differences) with decreasing the screening length, and (iii) change (decrease) of electronic couplings in the collision system with decreasing the screening length. The change of the number of bound states in the collision system available for specific state-selective processes when the screening length varies, plays the most important role in the collision dynamics. This property of the potential screening can be used to control the number of reaction channels for a given process by varying the strength of the screening (e.g., by varying T_e and/or n_e in the Debye plasma). The decrease of binding energy of electronic states when the screening increases (λ_D decreases) should have an important impact on the ionization dynamics (by increasing

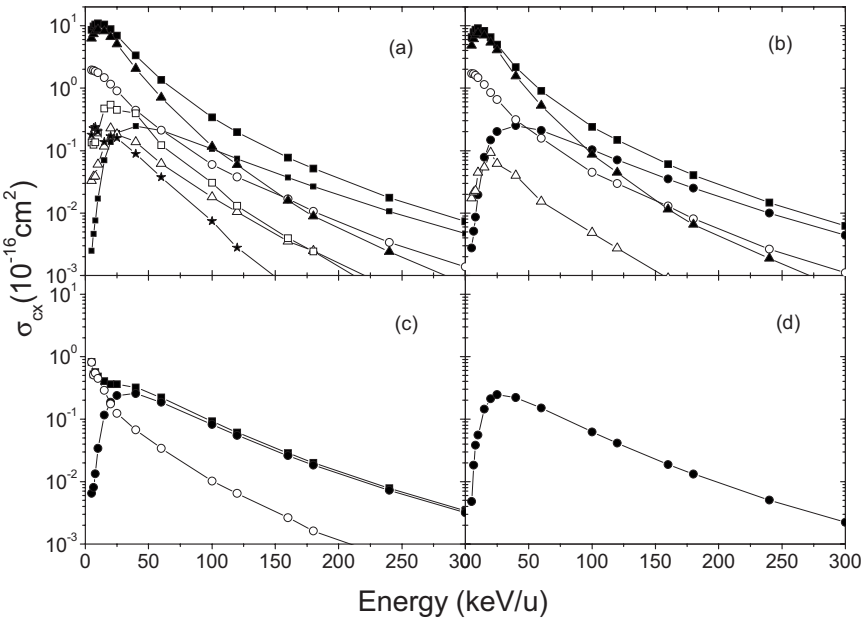

FIG. 9. Energy dependence of state-selective cross sections for electron capture to He^+ (nl) states, $n \leq 3$ for screened Coulomb potentials with $\lambda_D=6.0$, 4.0, 2.0, and $1.5a_0$ [(a)–(d), respectively] and their sum. The symbols are summed cross sections: filled squares; $1s$: filled circles; $2s$: open circles; $2p$: filled triangles; $3s$: open triangles; $3p$: open squares; and $3d$: filled stars. The lines connecting the calculated points are to guide the eye.

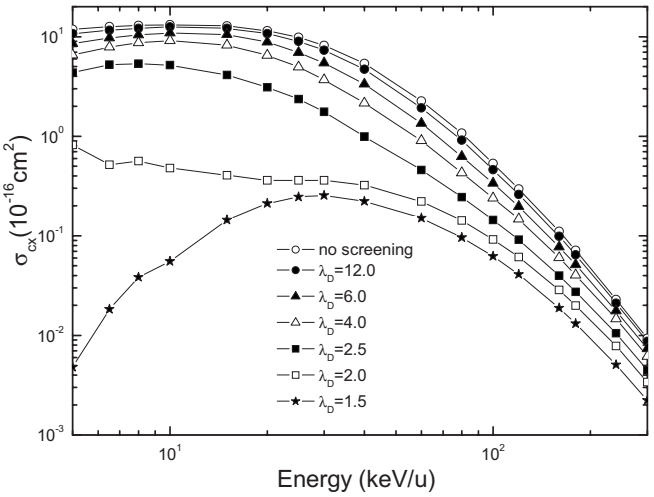

FIG. 10. Total electron-capture cross sections for reaction (2) with and without screening. The degree of screening is indicated by the value of λ_D. The lines connecting the calculated points are to guide the eye.

the coupling of discrete and continuum states). The ionization dynamics in ion-atom collisions will be discussed in a separate paper. Furthermore, since the difference $\Delta E_{nl,n'l'}$ of $E_{nl}(\lambda_D)$ and $E_{n'l'}(\lambda_D)$ atomic energy levels also depends on λ_D, the variation of parameters on which λ_D depends (T_e and n_e of a Debye plasma) will have dramatic effects on the radiative transitions between screened nl and $n'l'$ states (line shift and broadening).

Although the above conclusions about the effects of screened Coulomb interactions on the dynamics of ion-atom collision processes have been derived from the study of $He^{2+}+H(1s)$ collision dynamics, it is clear that they should be valid for any one-electron (or "one-active electron") collision system as long as the interaction has the form of Eq. (3). On the basis of the short range character of the interaction (3) and its property to support only a finite number of bound states, one can expect that even in the many-electron systems the reduction of the number of bound states will take place with increasing the screening and thus will affect the collision dynamics. The energy decrease of the lowest bound s states in a number of He-like ions, and their entering the continuum at certain $\lambda_{D,c}^{n,l}$, has been demonstrated in Ref. [38].

ACKNOWLEDGMENTS

One of the authors (R.K.J) would like to acknowledge the warm hospitality of the Institute of Applied Physics and Computational Mathematics during the period when this work was performed. We thank C. D. Lin for use of his AOCC code. This work is partly supported by the National Natural Science Foundation of China (Grants No. 10574018 and No. 10574020).

[1] J. C. Weisheit, in *Applied Atomic Collision Physics*, edited by C. F. Barnett and M. F. A. Harrison (Academic, New York, 1984), Vol. 2.
[2] J. C. Weisheit, Adv. At. Mol. Phys. **25**, 101 (1988).
[3] M. S. Murillo and J. C. Weisheit, in *Strongly Coupled Plasma Physics*, edited by H. M. Van Horn (University of Rochester Press, Rochester, New York, 1993), p. 233.
[4] M. S. Murillo, in *Atomic Processes in Plasmas*, edited by A. L. Osterheld and W. H. Goldstein, AIP Conf. Proc. No. 381 (American Institute of Physics, New York, 1996), p. 231.
[5] J. Quant. Spectrosc. Radiat. Transf. **27**, 3 (1982). The entire issue is devoted to the radiation properties of hot, dense plasmas.
[6] E. L. Pollock and J. C. Weisheit, in *Spectral Line Shapes*, edited by F. Rostas (Walter de Gruyter, New York, 1985), Vol. 3, p. 181.
[7] A. V. Vinogradov and V. P. Shevelko, Sov. Phys. JETP **44**, 542 (1976).
[8] B. L. Whitten, N. F. Lane, and J. C. Weisheit, Phys. Rev. A **29**, 945 (1984); B. L. Whitten, N. F. Lane, and J. C. Weisheit, *ibid.* **30**, 650 (1984).
[9] J. K. Yuan, Y. S. Sun, and S. T. Zheng, J. Phys. B **29**, 153 (1996).
[10] Y.-D. Jung, Phys. Plasmas **2**, 332 (1995); **2**, 1775 (1995).
[11] Y.-D. Jung, Phys. Plasmas **4**, 21 (1997).
[12] Y.-D. Jung and J.-S. Yoon, J. Phys. B **29**, 3549 (1996).
[13] M. Rasolt and F. Perrot, Phys. Rev. Lett. **62**, 2273 (1989).
[14] K. Scheibner, J. C. Weisheit, and N. F. Lane, Phys. Rev. A **35**, 1252 (1987).
[15] C.-G. Kim and Y.-D. Jung, Phys. Plasmas **5**, 2806 (1998); **5**, 3493 (1998).
[16] Y.-D. Jung, Europhys. Lett. **69**, 753 (2005).
[17] H. Zhang, J. G. Wang, B. He, Y. B. Qiu, and R. K. Janev, Phys. Plasmas **14**, 053505 (2007).
[18] N. Bohr and J. Lindhard, K. Dan. Vidensk. Selsk. Mat. Fys. Medd. **28**, 1 (1954).
[19] G. M. Harris, Phys. Rev. **125**, 1131 (1962).
[20] J. P. Hansen and I. R. McDonald, *Theory of Simple Fluids* (Academic, London, 1986).
[21] S. Ichimaru, Phys. Rev. A **2**, 494 (1970).
[22] W. Fritsch and C. D. Lin, Phys. Rep. **202**, 1 (1991).
[23] W. Fritsch, R. Shingal, and C. D. Lin, Phys. Rev. A **44**, 5686 (1991).
[24] N. Toshima, Phys. Rev. A **50**, 3940 (1994).
[25] J. Kuang and C. D. Lin, J. Phys. B **30**, 101 (1997).
[26] T. G. Winter, Phys. Rev. A **37**, 4656 (1988).
[27] L. F. Errea, C. Harel, H. Jouin, J. M. Maidagan, L. Mendez, B. Pons, and A. Riera, Phys. Rev. A **46**, 5617 (1992).
[28] C. M. Reeves, J. Chem. Phys. **39**, 1 (1963).
[29] L. D. Landau and E. M. Lifshitz, *Quantum Mechanics: Non-Relativistic Theory* (Pergamon, London, 1958).
[30] R. Dutt, M. Bag, and Y. P. Varshni, J. Phys. B **21**, 927 (1988).
[31] P. Chandhury and S. Bhattacharya, Chem. Phys. Lett. **296**, 51 (1998).

[32] R. L. Greene and C. Aldrich, Phys. Rev. A **14**, 2363 (1976).
[33] C. Stubbins, Phys. Rev. A **48**, 220 (1993).
[34] H. M. Schey and J. L. Schwartz, Phys. Rev. **139**, B1428 (1965).
[35] F. J. Rogers, H. C. Graboske, and D. J. Harwood, Phys. Rev. A **1**, 1577 (1970).
[36] R. K. Janev, J. Pop-Jordanov, and E. A. Solov'ev, J. Phys. B **30**, L353 (1997).
[37] P. S. Krstić, C. O. Reinhold, and D. R. Schnltz, J. Phys. B **31**, L155 (1998).
[38] T. Hashino, S. Nakazaki, T. Kato, and H. Kashiwabara, Phys. Lett. A **123**, 236 (1987).